we obtain for the spectral density of fractional frequency fluctuations, $S_y(f) = (f/\nu_0)^2 S_{\varphi o}(f)$:

$$S_y(f) = 2\times 10^{-10}\left[\frac{f}{\nu_0^2} + \frac{1}{4Q^2 f}\right]. \tag{2}$$

The Allan variance, σ_y^2, is given approximately by [9]

$$\sigma_y^2(\tau) = \left(\frac{10^{-15}}{\tau}\right)^2 + \left(\frac{8.3\times 10^{-6}}{Q}\right)^2 \tag{3}$$

for a measuring time τ, using an oscillator frequency of 8.5 GHz and a bandwidth of 1 kHz. We see from (3) that using a resonator with a loaded Q of 10^9 (easily possible with present-day superconducting technology), one would expect to obtain fractional frequency fluctuations $\sigma_y = \Delta f/f$ of $\sim 8.3\times 10^{-15}$ for times longer than 0.5 s. For shorter times the first term on the right-hand side of (3) becomes important. Since the oscillator would run at a power level of ~ 1 mW, thermal noise would not make a significant contribution to the Allan variance for measuring times longer than 0.5 s.

In comparison with this prediction, the frequency sources with the best short-term stability presently available commercially are quartz crystal oscillators, and the best of these exhibit fractional frequency fluctuations $\Delta f/f$ of $\sim 2\times 10^{-13}$ for 1 s $< \tau < 100$ s.

We are presently building a cooled loop oscillator using the 8.5 GHz amplifier in order to test our prediction.

V. Conclusions

We have measured the phase noise of an 8.5 GHz GaAs MESFET amplifier at temperatures from 1.7 K to 300 K. The observed flicker phase noise was found to vary only weakly with amplifier bias conditions and input power level, even when operating well past the 1 dB gain compression point. A cryogenic loop oscillator based on an amplifier with the level of intrinsic phase noise we observed at 2 K should have exceptionally good short-term frequency stability.

References

[1] S Weinreb, "Low-noise cooled GASFET amplifiers," *IEEE Trans Microwave Theory Tech*, vol. MTT-28, pp. 1041–1054, Oct 1980.

[2] B Hughes, N. G. Fernandez, and J M. Gladstone, "GaAs FET's with a flicker-noise corner below 1 MHz," *IEEE Trans. Electron Devices*, vol ED-34, pp. 733–741, Apr. 1987.

[3] R A. Pucel and J. Curtis, "Near-carrier noise in FET oscillators," in *1983 IEEE MTT-S Int. Microwave Symp. Dig*, pp. 282–284.

[4] A. N. Riddle and R. J. Trew, "A novel GaAs FET oscillator with low phase noise," in *1985 IEEE MTT-S Int Microwave Symp Dig.*, pp. 257–260.

[5] H. J Siweris and B. Schiek, "Analysis of noise upconversion in microwave FET oscillators," *IEEE Trans. Microwave Theory Tech*, vol. MTT-33, pp. 233–242, Mar. 1985.

[6] L. D Mann, D. G. Blair, and K. J. Wellington, "Flicker noise in GaAs MESFET *X*-band amplifiers in the temperature range 300 K to 2 K," *Electron Lett*, vol. 22, pp 1037–1038, Sept. 1986

[7] M G Richards, A. R. Andrews, C. P Lusher, and J Schratter, "Cryogenic GaAs FET amplifiers and their use in NMR detection," *Rev Sci Instrum* vol. 57, pp. 404–409, Mar. 1986.

[8] M. D. Hürlimann and W N. Hardy, "Measurement of flicker phase noise of 1.4 GHz MESFET amplifier at temperatures between 300 K and 1.26 K," *Electron Lett.*, vol. 23, pp. 283–284, Mar. 1987.

[9] S R. Stein, "Frequency and time—Their measurement and characterization," in *Precision Frequency Control* vol. 2, E. A Gerber and A Ballato, Eds. Orlando: Academic Press, 1985

[10] F. L. Walls and C M. Felton, "Low noise frequency synthesis," in *Proc 41st Ann. Freq. Contr Symp*, 1987, pp. 512–518.

[11] D B Leeson, "Simple model of feedback oscillator noise spectrum," *Proc IEEE*, vol 54, pp. 329–330, Feb. 1966.

[12] G Sauvage, "Phase noise in oscillators: A mathematical analysis of Leeson's model," *IEEE Trans. Instrum. Meas.*, vol IM-26, pp. 408–410, Dec 1977

Determination of the Scattering Matrix of Ring-Loaded Corrugated Waveguide Mode Converters

LUIZ C. DA SILVA

***Abstract*—A previously developed method for the determination of the scattering matrix of cylindrical waveguide mode converters, which is based on the representation of the fields inside the corrugations by a small number of radial modes, is extended to mode converters with ring-loaded corrugations. The method, besides being accurate, reduces the computer time necessary for the computations.**

I. Introduction

Cylindrical waveguide mode converters, composed of a section of nonuniform corrugated waveguide, are employed as a matching device between smooth-walled input waveguides and corrugated horns, transforming the fundamental mode of the input waveguide into the desired mode of the horn [1], [2].

In a previous work [3] a method was developed for the determination of the scattering matrix of such converters. The method is based on the representation of the fields inside the corrugations by a small number of radial modes. In the present paper, this technique is extended to include converters with ring-loaded corrugations.

The main benefit resulting from the use of ring-loaded corrugations is an increase in the bandwidth of the converter.

A method of analysis for ring-loaded converters was previously developed by James and Thomas [2] on the basis of mode-matching techniques and the expansion of the fields inside the waveguide sections into modes propagating along the axis of the converter. The advantage of the present formulation is the saving of computer time it affords without loss of accuracy in the results.

II. Formulation of the Problem

The overall scattering matrix of the converter is obtained by dividing the structure into elementary sections, as shown in Fig. 1(a), calculating the scattering matrix of each section, and progressively cascading them. The scattering matrix of an elementary section is determined by following these steps:

(i) The elementary section is decomposed into three cascaded subsections, as shown in Fig. 1(b). Subsection I is the discontinuity between two smooth-walled waveguides, and subsection III is formed by a smooth-walled waveguide of length l. The scattering matrices of these subsections are calculated according to [1].

(ii) To obtain the scattering matrix of subsection II, it is initially transformed into the equivalent structure shown in Fig. 1(c), where metallic walls and magnetic surface current densities, $\pm \vec{M}_1$ and $\pm \vec{M}_2$, were placed at $\rho = b$ and $\rho = c$. In this way the

Manuscript received June 1, 1988, revised September 30, 1988 This work was supported in part by TELEBRÁS S A (Brazilian Telecommunications Agency) under Contract 168/86-JPqD

The author is with the Pontifícia Universidade Católica do Rio de Janeiro, Rio de Janeiro, Brazil

IEEE Log Number 8825392

0018-9480/89/0300-0646$01.00 ©1989 IEEE

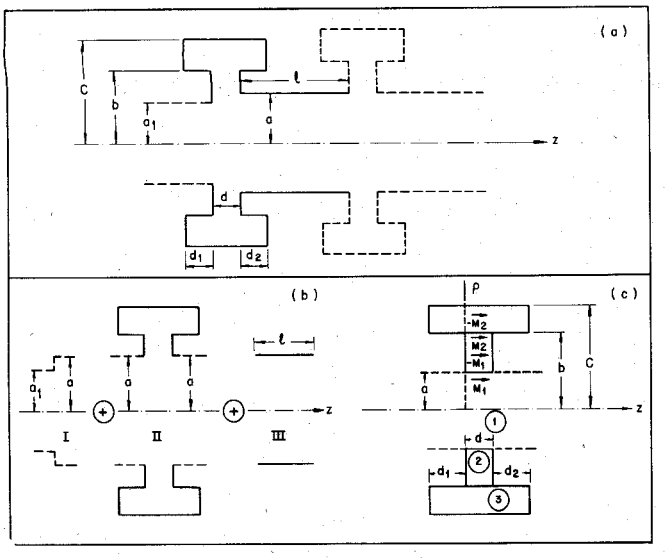

Fig. 1. An elementary section of a mode converter.

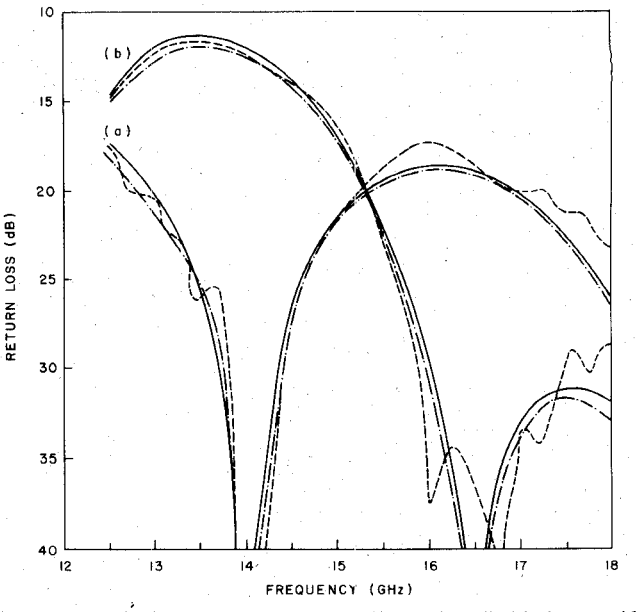

Fig. 2. Return loss, as a function of frequency, for the cylindrical waveguide sections with three ring-loaded corrugations shown in [2, fig. 5(a) and (b)]. (———) Theoretical results applying the present method (using 12 modes in region 1, four modes in region 2, and six modes in region 3); (–·–·–) theoretical results applying the method given in [2] (taking eight modes at the input waveguide); (– – –) experimental results according to [2]. Curves (*a*) correspond to the waveguide shown in [2, fig. 5(a)] and curves (*b*) correspond to the waveguide shown in fig. 5(b) of the same reference.

subsection is divided into three regions: region 1 is a smooth-walled waveguide of radius a and length d; regions 2 and 3 are cavities limited by the surfaces $\rho = a$, $\rho = b$, $z = 0$, $z = d$ and $\rho = b$, $\rho = c$, $z = -d_1$, $z = d + d_2$, respectively.

The subsection is excited by an incident wave composed of a summation of modes (TE_{1n} and TM_{1n}) of the smooth-walled waveguide of radius a.

The magnetic surface current densities due to the nth mode of the incident wave are given by

$$\vec{M}_{1_n} = \vec{a}_\rho \times \vec{E}_2(a) \cdots \tag{1a}$$

$$\vec{M}_{2_n} = \vec{a}_\rho \times \vec{E}_2(b) \cdots \tag{1b}$$

where $\vec{a}_\rho$ is the unit vector in the ρ direction and $\vec{E}_2(x)$ is the electric field effectively existing in region 2, at $\rho = x$.

Expanding $\vec{E}_2$ into a summation over the radial modes, TE_{n1} and TM_{n1} for the parallel-plate waveguide defined by the planes $z = 0$ and $z = d$, $\vec{e}_p^{\,TE}(\vec{r})$ and $\vec{e}_p^{\,TM}(\vec{r})$, respectively (given by [4, eqs. (5.18), (5.19), (5.33) and (5.35)], results in

$$\vec{M}_{1_n} = \sum_{p=0}^{PM} m_{1_{pn}}^M \left(k_{2_p}^2 \sin\phi \cos\alpha_{2_p} z \vec{a}_\phi + \frac{\alpha_{2_p}}{a} \cos\phi \sin\alpha_{2_p} z \vec{a}_z \right) + \sum_{p=1}^{PE} m_{1_{pn}}^E \cos\phi \sin\alpha_{2_p} z \vec{a}_z \cdots \tag{2a}$$

$$\vec{M}_{2_n} = \sum_{p=0}^{PM} m_{2_{pn}}^M \left(k_{2_p}^2 \sin\phi \cos\alpha_{2_p} z \vec{a}_\phi + \frac{\alpha_{2_p}}{b} \cos\phi \sin\alpha_{2_p} z \vec{a}_z \right) + \sum_{p=1}^{PE} m_{2_{pn}}^E \cos\phi \sin\alpha_{2_p} z \vec{a}_z \tag{2b}$$

where $\alpha_{2_p} = p\pi/d$, $k_{2_p}^2 = k_0^2 - \alpha_{2_p}^2$, k_0 is the free-space wavenumber, $\vec{a}_\phi$ and $\vec{a}_z$ are unit vectors in the directions ϕ and z, respectively, $m_{1_{pn}}^M$, $m_{1_{pn}}^E$, $m_{2_{pn}}^M$, and $m_{2_{pn}}^E$ are unknown coefficients, and the summations were truncated into PE TE and $PM+1$ TM modes.

(iii) The magnetic fields inside regions 1, 2, and 3 as a function of the unknown coefficients $m_{1_{pn}}^M$, $m_{1_{pn}}^E$, $m_{2_{pn}}^M$, and $m_{2_{pn}}^E$ are determined with the help of the magnetic dyadic Green's functions of the corresponding regions:

$$\vec{H} = \int_s \overline{\overline{G}}(\vec{r}, \vec{r}') \cdot \vec{M}(\vec{r}')\, ds' \tag{3}$$

where $\vec{M}(\vec{r}')$ means $\vec{M}_{1_n}$ or $\vec{M}_{2_n}$.

The expressions for $\overline{\overline{G}}(\vec{r}, \vec{r}')$ and for $\vec{M}_{1_n}$ and $\vec{M}_{2_n}$ are given in [3, eqs. (A.1) and A(2)] and by (2), respectively.

(iv) The boundary conditions for the magnetic fields at $\rho = a$ and $\rho = b$ yield

$$\vec{H}_{in}^T(a) + \vec{H}_{wg}^T(a) = \vec{H}_2^T(a) \tag{4a}$$

$$\vec{H}_2^T(b) = \vec{H}_3^T(b). \tag{4b}$$

Here, $\vec{H}_{in}^T(x)$, $\vec{H}_{wg}^T(x)$, $\vec{H}_2^T(x)$, and $\vec{H}_3^T(x)$ denote components transverse to ρ at $\rho = x$ of the magnetic fields incident into the subsection and in regions 1, 2, and 3, respectively.

Vector multiplying both members of (4a) and (4b), the first by $\vec{e}_p^{\,TE}(a)$, $p = 1,2,\cdots, PE$, and by $\vec{e}_p^{\,TM}(a)$, $p = 0,1,2,\cdots, PM$, and the second by $\vec{e}_p^{\,TE}(b)$, $p = 1,2,\cdots, PE$, and by $\vec{e}_p^{\,TM}(b)$, $p = 0,1,2,\cdots, PM$, and integrating the resulting expressions over the surfaces $0 \leqslant z \leqslant d$, $\rho = a$ and $0 \leqslant z \leqslant d$, $\rho = b$, respectively, the following system of linear equations is obtained:

$$\left[\overline{\overline{Q}}\right] = \left[\overline{\overline{M}}\right]\left[\overline{\overline{H}}_{in}\right]. \tag{5}$$

Here $\overline{\overline{Q}}$ is a $2(PE + PM + 1) \times 2(PE + PM + 1)$ matrix; $\overline{\overline{M}}$ is a $2(PE + PM + 1) \times (NE + NM)$ matrix containing the coefficients $m_{1_{pn}}^E$, $m_{1_{pn}}^M$, $M_{2_{pn}}^E$, and $m_{2_{pn}}^M$; $NE(NM)$ is the number of TE (TM) modes considered as composing the incident wave; and $\overline{\overline{H}}_{in}$ is a $2(PE + PM + 1) \times (NE + NM)$ matrix. Expressions for the elements of $\overline{\overline{Q}}$ and $\overline{\overline{H}}_{in}$ are given in the Appendix.

Inverting (5), the coefficients $m_{1_{pn}}^E$, $m_{1_{pn}}^M$, $m_{2_{pn}}^E$, and $m_{2_{pn}}^E$ are obtained.

(v) Once $m_{1_{pn}}^E$ and $m_{1_{pn}}^M$ are known, the elements of the scattering matrix of the subsection under consideration are obtained from [3, eqs. (12.a) to (12.d)], substituting into these equations $m_{1_{pn}}^E$ and $m_{1_{pn}}^M$ for m_{pn}^E and m_{pn}^M, respectively.

III. Numerical Results

As an example of an application, the method proposed here was applied to the determination of the scattering matrices of the cylindrical waveguides sections with the three ring-loaded corrugations shown in [2, figs. 5(a) and 5(b)]. Theoretical results for the return loss are shown in Fig. 2. Also shown in the same figure are the theoretical results obtained using the method given in [2], together with the experimental results according to [2]. Discrepancies between theoretical results are less than 1 dB. The present method of calculation reduced computer time by a factor of 4.

IV. Conclusions

The utilization of radial modes in the characterization of the fields inside the corrugations of ring-loaded cylindrical waveguide mode converters has permitted the development of a technique for determining the scattering matrix of these converters. The main advantages of this technique are its accuracy and computer time economy.

Appendix
Expressions for the Elements of $\overline{\overline{Q}}$ and $\overline{\overline{H}}_{in}$

The expressions for elements of the matrices $\overline{\overline{Q}}$ and $\overline{\overline{H}}_{in}$, calculated according to the procedure given in Section II, are as follows.

Elements of $\overline{\overline{Q}}$:

$$q_{i,j} = \text{given by [3, eq. (A.10) to (A.13)]}, \quad i=1,PT;\ j=1,PT \tag{A1}$$

$$q_{i,j+PT} = 2C_i^E(a,a)\delta_{ij}, \quad i=1,PE;\ j=1,PE \tag{A2}$$

$$q_{i+PE+1,j+PT1} = 2C_i^M(a,a)\epsilon_i\delta_{ij}, \quad i=0,PM;\ j=0,PM \tag{A3}$$

$$q_{i+PT,j} = -C_i^E(b,b)\delta_{ij}, \quad i=1,PE;\ j=1,PE \tag{A4}$$

$$q_{i+PT,j+PT} = -C_i^E(b,a)\delta_{ij} - \sum_{k=1}^{PE} F_2(j,k)\gamma_2(i,k), \quad i=1,PE;\ j=1,PE \tag{A5}$$

$$q_{i+PT,j+PT+1} = \sum_{k=1}^{PE} F_3(j,k)\gamma_2(i,k), \quad i=1,PE;\ j=0,PM \tag{A6}$$

$$q_{i+PT1,j+PE+1} = -C_i^M(b,b)\epsilon_i\delta_{ij}, \quad i=0,PM;\ j=0,PM \tag{A7}$$

$$q_{i+PT1,j+PT} = \sum_{k=1}^{PE} F_2(j,k)\left[\frac{\alpha_{2_i}}{b}\gamma_2(i,k) - \frac{\alpha_{3_k}}{b}\gamma_1(i,k)\right], \quad i=0,PM;\ j=1,PE \tag{A8}$$

$$q_{i+PT1,j+PT1} = -C_i^M(b,a)\epsilon_i\delta_{ij} + \sum_{k=1}^{PE} F_3(j,k)\cdot\left[\frac{\alpha_{3_k}}{b}\gamma_1(i,k) - \frac{\alpha_{2_i}}{b}\gamma_2(i,k)\right] - \sum_{p=0}^{PM} F_1(j,k)\gamma_1(i,k), \quad i=0,PM;\ j=0,PM \tag{A9}$$

$$q_{i,j} = 0 \quad \text{if not defined above.} \tag{A10}$$

Here

$$PT = PE + PM + 1 \qquad PT1 = PT + PE + 1$$

$$\delta_{ij} = \begin{cases} 1 & \text{if } i=j \\ 0 & \text{if } i\neq j \end{cases}$$

$$\epsilon_i = \begin{cases} 2 & \text{if } i=0 \\ 1 & \text{if } i\neq 0 \end{cases}$$

$$C_p^M(x,y) = \frac{jk_0}{2Z_0}k_{2_p}^2 d \cdot \frac{J_1'(k_{2_p}x)H_1^{(2)}(k_{2_p}y) - J_1(k_{2_p}y)H_1^{(2)\prime}(k_{2_p}x)}{J_1(k_{2_p}b)H_1^{(2)}(k_{2_p}a) - J_1(k_{2_p}a)H_1^{(2)}(k_{2_p}b)}.$$

Z_0 is the free-space impedance; $J_1(x)$ is the Bessel function of the first kind of order 1; $H_1^{(2)}(x)$ is the Hankel function of the second kind of order 1; and $J_1'(kx) = d[J_1(kx)]/dx$; $H_1^{(2)\prime}(kx) = d[H_1^{(2)}(kx)/dx]$

$$C_P^E(x,y) = \frac{j}{2k_0Z_0}k_{2_p}^2 d \cdot \frac{J_1(k_{2_p}x)H_1^{(2)\prime}(k_{2_p}y) - J_1'(k_{2_p}y)H_1^{(2)}(k_{2_p}x)}{J_1'(k_{2_p}b)H_1^{(2)\prime}(k_{2_p}a) - J_1'(k_{2_p}a)H_1^{(2)\prime}(k_{2_p}b)}$$

$$\alpha_{2_p} = p\pi/d \qquad k_{2_p}^2 = k_0^2 - \alpha_{2_p}^2$$

$$\alpha_{3_p} = q\pi/(d+d_1+d_2) \qquad k_{3_q}^2 = k_0^2 - \alpha_{3_q}^2$$

$$\gamma_1(p,q) = k_{2_p}^2\int_0^d \cos\alpha_{2_p}z\cos\alpha_{3_q}(z+d_1)\,dz$$

$$\gamma_2(p,q) = k_{3_q}^2\int_0^d \cos\alpha_{2_p}z\sin\alpha_{3_q}(z+d_1)\,dz$$

$$F_1(p,q) = \frac{2jk_0}{Z_0k_{3_q}^2d_2\epsilon_i} \cdot \frac{J_1'(k_{3_q}b)H_1^{(2)}(k_{3_q}c) - J_1(k_{3_q}c)H_1^{(2)\prime}(k_{3_q}b)}{J_1(k_{3_q}c)H_1^{(2)}(k_{3_q}b) - J_1(k_{3_q}b)H_1^{(2)}(k_{3_q}c)} \cdot\gamma_1(p,q)$$

$$F_2(p,q) = \frac{2j}{k_0Z_0d_2k_{3_q}^2} \cdot \frac{J_1(k_{3_q}b)H_1^{(2)\prime}(k_{3_q}c) - J_1'(k_{3_q}c)H_1^{(2)}(k_{3_q}b)}{J_1'(k_{3_q}c)H_1^{(2)\prime}(k_{3_q}b) - J_1'(k_{3_q}b)H_1^{(2)\prime}(k_{3_q}c)} \cdot\gamma_2(p,q)$$

$$F_3(p,q) = \frac{2j}{k_0Z_0d_2k_{3_q}^2b} \cdot \frac{J_1(k_{3_q}b)H_1^{(2)\prime}(k_{3_q}c) - J_1'(k_{3_q}c)H_1^{(2)}(k_{3_q}b)}{J_1'(k_{3_q}c)H_1^{(2)\prime}(k_{3_q}b) - J_1'(k_{3_q}b)H_1^{(2)\prime}(k_{3_q}c)} \cdot\gamma_3(p,q).$$

Here

$$\gamma_3(p,q) = \alpha_{3_q}\gamma_1(p,q) - \alpha_{2_p}\gamma_2(p,q).$$

Elements of $\overline{\overline{H}}_{in}$:

$$h_{in_{i,j}} = \text{given by [3, eqs. (A.14) to (A.17)]},$$

$$i = 1, PT;\ j = 1, NE + NM \quad \text{(A11)}$$

$$h_{in_{i,j}} = 0 \quad \text{if not defined above.} \quad \text{(A12)}$$

REFERENCES

[1] G. L. James, "Analysis and design of TE_{11}-to-HE_{11} corrugated cylindrical waveguide mode converters," *IEEE Trans. Microwave Theory Tech.*, vol MTT-29, pp. 1059–1066, Oct. 1981.

[2] G. L. James and B. M. Thomas, "TE_{11}-to-HE_{11} cylindrical waveguide mode converters using ring-loaded slots," *IEEE Trans. Microwave Theory Tech.*, vol. MTT-30, pp. 278–285, Mar. 1982.

[3] L. C. da Silva, "A method of analysis TE_{11}-to-HE_{11} mode converters," *IEEE Trans. Microwave Theory Tech.*, vol. MTT-36, pp. 480–488, Mar. 1988.

[4] R. F. Harrington, *Time-Harmonic Electromagnetic Fields*. New York: McGraw-Hill, 1961.